applied sciences

MDPI

Article

Predictions of Ship Extreme Hydroelastic Load Responses in Harsh Irregular Waves and Hull Girder Ultimate Strength Assessment

Jialong Jiao [1], Yong Jiang [1], Hao Zhang [2], Chengjun Li [3] and Chaohe Chen [1,*]

1 School of Civil Engineering and Transportation, South China University of Technology, Guangzhou 510641, China; jiaojl@scut.edu.cn (J.J.); yong.bill.jiang@outlook.com (Y.J.)
2 Xi'an Benyong Information Technology Limited Company, Xi'an 710048, China; ky2012sj@163.com
3 Marine Design & Research Institute of China, Shanghai 200011, China; 13166035346@163.com
* Correspondence: chenchaohe@scut.edu.cn; Tel.: +86-153-2228-1331

Received: 19 December 2018; Accepted: 3 January 2019; Published: 10 January 2019

Abstract: In this paper, the hydroelastic motion and load responses of a large flexible ship sailing in irregular seaways are predicted and the hull girder ultimate strength is subsequently evaluated. A three-dimensional time-domain nonlinear hydroelasticity theory is developed where the included nonlinearities are those arising from incident wave force, hydrostatic restoring force and slamming loads. The hull girder structure is simplified as a slender Timoshenko beam and fully coupled with the hydrodynamic model in a time domain. Segmented model towing-tank tests are then conducted to validate the proposed hydroelasticity theory. In addition, short-term and long-term predictions of ship responses in irregular seaways are conducted with the help of the developed hydroelastic code in order to determine the extreme design loads. Finally, a simplified strength-check equation is proposed, which will provide significant reference and convenience for ship design and evaluation. The hull girder ultimate strength is assessed by both the improved Rule approach and direct calculation.

Keywords: ship hydrodynamics; hydroelasticity theory; wave loads; slamming loads; irregular waves; ultimate strength

1. Introduction

Accurately predictions of ship hydrodynamics and wave-induced loads are the fundamental work for hull structural strength assessment. In the past decades, considerable efforts have been made to investigate the seakeeping performance and wave load response of ships, which includes two-dimensional (2D) strip theory [1,2], three-dimensional (3D) panel theory [3] and 2.5D high speed slender body theory [4]. For the cases of rigid ships the structural deformation is negligible during the determination of hydrodynamic responses. However, with the increasing demand for large-dimension high-speed ships, the structural deformation of flexible ships can no longer be ignored and the hydroelastic effects should be considered during the hydrodynamic and wave load calculations [5].

The hydroelasticity theory, which was first proposed in the field of aerodynamics [6], considers the effects of mutual interaction among inertial force, hydrodynamic force and elastic force [7]. Ship hydroelasticity theory has been widely developed in the community of Naval Architecture and Ocean Engineering (NAOE) since the 1970s [8]. The 2D hydroelasticity theory combines the strip theory with linear beam theory [9]. The 3D hydroelasticity theory combines the 3D potential flow theory with 1D beam theory or 3D structural finite element method (FEM) [10]. A comprehensive review of ship hydroelasticity theory, which includes 2D (or 3D) linear (or nonlinear) frequency-domain (or time-domain) methods can be found in [11]. The influence of different levels of nonlinearities, which includes linear, Froude–Krylov nonlinear, body nonlinear, body exact and smooth waves methods, on symmetric hydrodynamic responses for a ship operating in harsh waves with large amplitude motions can be found in References [12,13]. On the other hand, although the computational fluid dynamics (CFD) tool, which is on the basis of solving Reynolds Averaged Navier–Stokes (RANS) equations has been incorporated into the methodology of hydroelasticity, the immensity of time cost still makes it stay at early stage and far from practical engineering application [14]. Therefore, the potential flow theory constitutes an invaluable tool in the prediction of ships hydroelastic responses.

Large vessels with pronounced flare bow sailing in harsh weather are more susceptible to frequent and harsh wave impacts, which will result in large increase of transient hull girder vibration loads called whipping. The slamming induced whipping loads are primarily an ultimate strength issue and it decays rapidly due to the structural damping effects [15]. Moreover, the springing responses of hull girder occur even in low wave states and it may last for a considerable long time once excited. The magnitude of springing loads is usually low; however, the number of cycles can be very large, which highly contribute to the fatigue damage of the structure [16]. The time-domain hydroelasticity theory sufficiently considers the effects of structural responses on the hydrodynamic forces and therefore provides opportunities for the investigation of whipping and springing loads. Hong and Kim [17] investigated the springing and whipping characteristics of a large container ship by segmented flexible model tank experiments. Kim et al. [18] developed a fully coupled hydroelastic model which combine a 3D Rankine panel method, a 1D or 3D FEM, and a 2D Generalized Wagner Model (GWM). Southall et al. [19] conducted a comparative and benchmark study on the impact loads predicted by using CFD tools OpenFOAM and STAR-CCM+ with experimental data.

To date, majority of the literature work are focusing on the investigation of ship hydroelastic responses in regular waves [20–22]. However, the realistic irregular waves are much more complex compared with the regular waves and they are associated with strongly nonlinearity and randomicity. Rajendran et al. [23] studied the effects of bow flare variation on the vertical responses of bulk carrier, containership and passenger ship in abnormal waves and extreme irregular seas. Wang and Soares [24] studied the slamming load characteristics of a chemical tanker in irregular waves experimentally and numerically. Kim and Kim [25] predicted the extreme loads on ultra-large containerships with structural hydroelasticity. In the authors' previous work [26], a 3D time-domain nonlinear hydroelasticity theory was developed to predict ship motion and load responses in regular waves; and the proposed hydroelasticity theory is extended to irregular wave case in this paper.

In fact, ships are subjected to a wide variety of different sea states during their whole lifetime, and the cycle times of alternate loads may be very large. Therefore, long-term prediction of wave-induced hull girder loads considering the effect of various operational circumstances is of great importance for the determination of the extreme design loads and the subsequent ultimate strength assessment. Soares et al. [27] assessed the maximum wave-induced loads occurred on a fast monohull during its lifetime by long-term distribution calculations of nonlinear vertical bending moment (VBM) amidship. Baarholm and Moan [28] developed a simplified algorithm for the estimation of long-term extreme value by identifying the most important sea states with limited number. Wu and Hermundstad [29] presented a nonlinear time-domain formulation for ship motions and loads estimation and also extended with a nonlinear long-term statistics method.

The wave load response of ship in harsh or extreme irregular waves and the structural safety is a special reason of concern. Since ships operate in unknown severe and high-risk environments, marine accidents due to structure failure may occur at seas. For example, on 18 January 2007, the 275-m-long containership MSC NAPOLI was caught in stormy weather and suffered severe structural damage and the crew were forced to abandon the ship and escaped with the help of helicopter (see Figure 1a). Another example may be the five-year-old 8100-TEU containership MOL COMFORT who broke in two in rough weather off Yemen on 17 June 2013 (see Figure 1b). In order to properly evaluate the hull structural strength and safety, in the recent years the International Association of

Classification Societies (IACS) stressed the contribution of whipping loads to extreme loads and its influence on hull girder ultimate strength by revising the chapter URS11A [30]. Mohammed et al. [31] presented a direct calculation method for the assessment of the ultimate strength of a 10,000 TEU container ship and the margin of safety between the ultimate capacity and the maximum expected moment is established. The China Classification Society (CCS) issued calculation guidance notes that evaluate the effects of whipping and springing loads on hull structural fatigue strength [32]. The CCS also plans to issue calculation guidance notes for assessing the effects of whipping and springing loads on hull structural ultimate strength. The work involved in this study is conducted in collaboration with CCS for such purpose of investigation.

(**a**) (**b**)

Figure 1. Structural failure of hull structures. (**a**) MSC NAPOLI; (**b**) MOL COMFORT.

In this paper, a 3D time-domain nonlinear hydroelasticity theory is presented to study the motion and load responses of a large flexible ship with pronounced bow flare in irregular waves. The hydrodynamic part is simulated by 3D potential flow theory and the structural part is addressed by 1D Timoshenko beam theory, and they are fully coupled by modal superposition method to consider the hydroelastic effects. The slamming loads calculated by momentum impact method are included into the hydroelastic motion equation. To validate the numerical results, experiments of a segmented ship model advancing in irregular head waves were carried out in a towing tank. In addition, short-term and long-term predictions of ship responses in irregular seaways are conducted with the help of the time-domain hydroelastic code in order to determine the extreme design loads. Based on the results obtained by direct calculation, a simplified ultimate strength check approach is proposed, which provides significance reference for ship design and evaluation by the Rule Book approach.

2. Ship Hydroelasticity Theory in Irregular Waves

2.1. Potential Flow Theory in Ship Hydroelasticity

The hydrodynamic part of ship hydroelastic equation is solved by 3D potential flow theory. Sketch of the ship wave interaction problem is shown in Figure 2. In the framework of potential flow theory, the fluid is assumed to be irrotational, inviscid and incompressible. The fluid domain is denoted as Ω_F and its boundary is composed of free surface boundary S_F, body surface boundary S_B, bottom boundary S_H and infinity radiation boundary S_∞. The ship is assumed to travel in waves with constant forward speed U. The angle between ship advancing direction and wave incoming direction is defined as wave heading angle β; i.e., 0°, 90°, 180° and 270° are heading wave, starboard beam wave, following wave and port beam wave, respectively.

Three Cartesian coordinate systems are introduced to describe the ship motion in waves. They are the space fixed system O-XYZ, the translational movement system o-xyz and the body fixed system G-$x_b y_b z_b$. The space fixed system O-XYZ is an earth absolutely coordinate system. The translational movement system *o-xyz* is moving horizontally with constant speed U and course angle β. The origins of these two coordinate systems are coincident initially. The body fixed system G-$x_b y_b z_b$ is fully fixed on the moving ship with its origin G coincides with the center of gravity (COG) of ship. The Galilean transformation relationship between the three coordinate systems is:

$$\begin{Bmatrix} x \\ y \\ z \end{Bmatrix} = \begin{bmatrix} \cos\beta & \sin\beta & 0 \\ -\sin\beta & \cos\beta & 0 \\ 0 & 0 & 1 \end{bmatrix} \begin{Bmatrix} X - Ut\cos\beta \\ Y - Ut\sin\beta \\ Z \end{Bmatrix} \approx \begin{Bmatrix} x_b \\ y_b \\ z_b + z_G \end{Bmatrix} \tag{1}$$

where t denotes time, z_G denotes the vertical height of COG of ship with respect to the undisturbed free surface.

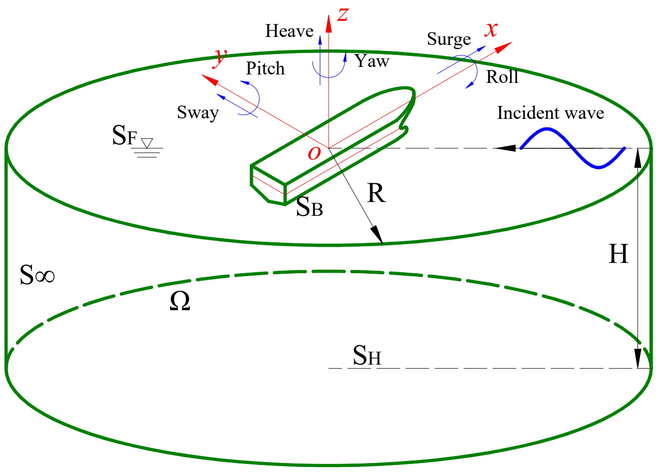

Figure 2. Description of ship–wave interaction issue.

The solution of velocity potential is based on the 3D boundary element method (BEM). The fluid disturbance velocity potential under the translational movement system *o-xyz* can be decomposed into:

$$\Phi(x, y, z, t) = \mathrm{Re}(\phi(x, y, z)e^{\mathrm{i}\omega_e t}) \tag{2}$$

where $\phi(x,y,z)$ is the space-dependent part of $\Phi(x,y,z,t)$, ω_e is wave encounter frequency which is defined as:

$$\omega_e = \omega\left(1 + \frac{U\omega}{g}\cos\beta\right) \tag{3}$$

where ω is the wave natural frequency, g is acceleration of gravity.

The spatial potential $\phi(x,y,z)$ can be further decomposed into:

$$\phi(x, y, z) = \zeta_a\phi_0(x, y, z) + \zeta_a\phi_d(x, y, z) + \sum_{r=1}^{m} p_{ra}\phi_r(x, y, z) \tag{4}$$

where ζ_a denotes amplitude of incident wave, ϕ_0 denotes incident wave potential under unit wave amplitude, ϕ_d denotes diffraction wave potential under unit wave amplitude, p_{ra} is the motion amplitude of the rth degree of freedom (DOF), ϕ_r denotes radiation wave potential under unit motion amplitude of the rth order DOF, when r = 1 − 6 it denotes rigid body 6-DOF motion and when r = 7 − m it denotes elastic deformation.

The incident wave potential ϕ_0 can be obtained by the incident wave field of regular waves directly, which is easy to obtain. The boundary value problem for the determination of radiation potential ϕ_r and diffraction potential ϕ_d in frequency-domain is expressed as follows:

$$\begin{cases} \nabla^2\phi_r = 0(in\ \Omega) \\ -\omega_e^2\phi_r + g\frac{\partial}{\partial z}\phi_r = 0(on\ z = 0) \\ \frac{\partial\phi_r}{\partial \mathbf{n}} = \begin{cases} (\mathrm{i}\omega_e\mathbf{u_r} - U\frac{\partial}{\partial x}\mathbf{u_r})\cdot\mathbf{n}(r = 1, 2, \cdots, m) \\ -\frac{\partial\phi_0}{\partial \mathbf{n}}(r = m+1) \end{cases} \quad (on\ S_B) \\ \begin{cases} \frac{\partial\phi_r}{\partial z} = 0(z = -H) \\ \nabla\phi_r = 0(z \to -\infty) \end{cases} \\ \lim\limits_{R\to\infty}\sqrt{R}(\frac{\partial\phi_r}{\partial R} - \mathrm{i}k\phi_r) = 0(R \to \infty) \end{cases} \tag{5}$$

where **n** is the unit normal vector and is defined as positive when pointing from the wet boundary surface into the ship interior, $\mathbf{u_r}$ denotes the *r*-th order mode vector of displacement or deformation of the hull.

2.2. Solution of Hydroelastic Motion Equation

The hydroelastic motion governing equation of ship advancing in waves can be expressed as follows:

$$[\mathbf{m}][\ddot{\mathbf{p}}] + [\mathbf{c}][\dot{\mathbf{p}}] + [\mathbf{k}][\mathbf{p}] = [\mathbf{F}_I] + [\mathbf{F}_S] + [\mathbf{F}_D] + [\mathbf{F}_R] + [\mathbf{F}_{SL}] + [\mathbf{F}_{GW}] \tag{6}$$

where $[\mathbf{m}]$, $[\mathbf{c}]$ and $[\mathbf{k}]$ are the generalized structural mass, damping and stiffness matrices, respectively; $[\mathbf{p}]$ denotes the generalized principal coordinate column matrix; the fluid force terms $[\mathbf{F}_I]$, $[\mathbf{F}_S]$, $[\mathbf{F}_D]$, $[\mathbf{F}_R]$, $[\mathbf{F}_{SL}]$ and $[\mathbf{F}_{GW}]$ on the right-hand side of Equation (6) are Froude–Krylov force, hydrostatic restoring force, diffraction force, radiation force, slamming load and green water load column matrices, respectively.

The structural dynamic part on the left-hand side of Equation (6) is solved based on the linear structural mechanics theory. The hydrodynamic part on the right-hand side of Equation (6) is solved by nonlinear fluid mechanics theory. The nonlinear effects are considered as a compromise between the calculation accuracy requirement and time cost. Therefore, the Froude–Krylov force, hydrostatic restoring force, slamming loads and green water loads are calculated on the instantaneous wetted surface of the ship to include the nonlinearities associated with hull geometry. In contrast, the diffraction force and radiation force, which are obtained by solving the free-surface Green function, are remain as linear and calculated on the mean wetted ship surface in calm water. The calculation of generalized fluid force is described as follows.

(1) Hydrostatic restoring force

The nonlinear hydrostatic restoring force acting on the elastic hull is calculated on the instantaneous wetted body surface:

$$F_S^r(t) = -\rho g \sum_{k=1}^{m} p_{ka} \iint\limits_{S(t)} \mathbf{n}\mathbf{u_r} w_k ds - \int\limits_{L} F_g(x) w_r(x) \mathrm{d}x (r = 1, 2, \cdots, m) \tag{7}$$

where $S(t)$ denotes the instantaneous wetted body surface of hull in waves, p_{ka} is the *k*-th order principal coordinate amplitude, w_k denotes the *k*-th order mode of vertical displacement of the hull, F_g denotes the sectional hull weight.

(2) Incident wave force

For ships sailing in irregular waves, the incident wave force is obtained by integrating the contribution of each component of regular wave with different wave frequency, amplitude and phase. The following equation is used to obtain the incident wave force induced by irregular waves:

$$F_I^r(t) = -\rho \sum_{i=1}^{M} \zeta_{ai} \iint\limits_{S(t)} \mathbf{n} \cdot \mathbf{u}_r \left(\mathrm{i}\omega_i - U\frac{\partial}{\partial x}\right)\phi_{0i} \mathrm{d}s (r = 1, 2, \cdots, m) \tag{8}$$

where ζ_{ai}, ω_i, ϕ_{0i} are the wave amplitude, frequency and incident potential of ith sub-wave component, respectively.

(3) Diffraction wave force

Since the diffraction wave force is calculated on the static mean wetted surface, the time-domain convolution integral method is used to obtain the diffraction wave force induced by irregular waves:

$$F_D^r(t) = \int_0^t h_D^r(t-\tau)\zeta(\tau)\mathrm{d}\tau(r = 1, 2, \cdots, m) \tag{9}$$

$$h_D^r(t) = \frac{1}{\pi}\int_0^\infty H_D^r(i\omega)e^{\mathrm{i}\omega t}\mathrm{d}\omega(r = 1, 2, \cdots, m) \tag{10}$$

where $h_D{}^r(t)$ is the impulse response function (IRF) of diffraction wave force for r-th mode of motion, and $H_D{}^r(\mathrm{i}\omega)$ is the frequency-domain response function of diffraction wave force for r-th mode of motion in regular waves.

(4) Radiation wave force

For ships in irregular waves, the wave memory effects resulted from the persistence of radiation waves generated by the ship's motion and its scattering of incident irregular waves play an import role in the determination of radiation wave force. The radiation wave force in irregular waves can be expressed as:

$$\mathbf{F_R}(t) = -[\mathbf{A}^\infty]\{\ddot{\mathbf{p}}(t)\} - [\mathbf{B}^\infty]\{\dot{\mathbf{p}}(t)\} - [\mathbf{C}^\infty]\{\mathbf{p}(t)\} - \int_0^t \mathbf{K}(\tau)p(t-\tau)d\tau \tag{11}$$

where the $[\mathbf{A}^\infty]$, $[\mathbf{B}^\infty]$ and $[\mathbf{C}^\infty]$ are infinite frequency added mass, damping coefficient and stiffness matrices caused by speed effects, $\mathbf{K}(\tau)$ is the retardation function matrix and its component $K_{rk}(\tau)$ can be calculated according to the Kramer–Kronig relation equation:

$$K_{rk}(\tau) = \frac{2}{\pi}\int_0^\infty B_{rk}(\omega)\cos(\omega\tau)d\omega \tag{12}$$

where $B_{rk}(\omega)$ is the damping coefficient in frequency-domain.

(5) Slamming loads

In this study, the slamming loads for a ship sailing in irregular waves are obtained by momentum impact theory. The slamming force is determined by the momentum changing rate of the fluid around the bow region, which is expressed as follows:

$$f_{slam}(x,t) = \frac{\mathrm{d}m_\infty(x)}{\mathrm{d}z}\left(\frac{\mathrm{d}w_{rel}(x,t)}{\mathrm{d}t}\right)^2 \tag{13}$$

where $m_\infty(x)$ is the sectional infinite frequency added mass, $w_{rel}(x,t)$ is the real-time hull vertical displacement relative to the incident wave elevation and its time derivative can be expressed as:

$$V_z(x,t) = \dot{w}_{rel}(x,t) = \sum_{r=1}^{m} w_r(x)p_r(t) - \zeta(x,t) \tag{14}$$

where $w_r(x)$ is the rth mode of ship vertical displacement or deformation.

Then the generalized slamming force can be obtained by:

$$F_{slam}^r(t) = \int_L f_{slam}(x,t)n_{wr}(x)\mathrm{d}x \tag{15}$$

where $n_{wr}(x)$ is r-th vertical component of coordinate of the unit normal vector $\mathbf{n}$.

(6) Green water loads

The green water loads on deck are also calculated based on the momentum impact theory. The vertical impact force due to the presence of green water on deck is expressed as:

$$f_{gw}^{r}(x,t) = \left(\frac{\partial m_{gw}}{\partial t}\right) w_r(x) + \left(g\cos p_5 + \frac{\partial w_r}{\partial t}\right) m_{gw} \tag{16}$$

where m_{gw} is the mass of the water on deck. Then the overall green water loads acting on the whole elastic hull can be obtained by integrating the 2D sectional force longitudinally in a similar manner as Equation (15).

For the solution of the hydroelastic motion equation of Equation (6), the fourth-order Runge-Kutta algorithm is adopted in the present study. Then based on the modal superposition principle, the time-domain displacement $w(x,t)$, vertical bending moment $M(x,t)$, and shear force $V(x,t)$ along ship length can be written as follows:

$$\begin{cases} w(x,t) = \sum\limits_{r=1}^{m} p_r(t) w_r(x) \\ M(x,t) = \sum\limits_{r=1}^{m} p_r(t) M_r(x) \\ V(x,t) = \sum\limits_{r=1}^{m} p_r(t) V_r(x) \end{cases} \tag{17}$$

where $w_r(x)$, $M_r(x)$ and $V_r(x)$ are the r-th mode of vertical displacement, vertical bending moment and shear force, respectively.

2.3. Prediction and Statistics of Extreme Values

The long-term statistics of wave-induced motions and loads is well established in linear frequency-domain theory. The short-term response of ship linear motion and load is a stationary Gaussian narrow-band process with zero mean, and therefore their peaks obey Rayleigh distribution. The long-term distribution is then obtained by superposition of short-term probabilities of exceedance in all possible combinations of wave states, heading angles, navigational speeds and loading conditions.

However, the nonlinear motion and load response is no longer Gaussian and the peak distribution cannot be described by Rayleigh distribution. Moreover, the hogging and sagging VBM reveal obvious asymmetry due to the effects of fluid dynamics and slamming loads. Therefore, the short-term statistics should be processed using time series analysis method rather than the spectral analysis method. The time series analysis method is described in Section 4.1 and the following statistical method is used to obtain the probability distribution of the counted peaks. Suppose the random variable X is of Weibull distribution, then the probability density function and cumulative distribution function of variable x, which represents the statistical peak values (e.g., crest or trough), can be, respectively, expressed as follows:

$$f_0(x) = \frac{l}{k}\left(\frac{x}{k}\right)^{l-1} e^{-\left(\frac{x}{k}\right)^{l}} \tag{18}$$

$$F_0(x) = 1 - e^{-\left(\frac{x}{k}\right)^{l}} \tag{19}$$

where l and k are the two parameters of Weibull distribution.

Suppose that the loading condition of ship does not change, the probability density function and cumulative distribution function for long-term prediction can be obtained by summation of short-term results in all possible combinations of the independent wave states, heading angles and navigational speeds:

$$f(x) = \frac{\sum\limits_i \sum\limits_j \sum\limits_k n_0^{ijk} p_i(H_{1/3}, T_z) p_j(\beta) p_k(U) f_0^{ijk}(x)}{\sum\limits_i \sum\limits_j \sum\limits_k n_0^{ijk} p_i(H_{1/3}, T_z) p_j(\beta) p_k(U)} \tag{20}$$

$$F(x) = \frac{\sum\limits_i \sum\limits_j \sum\limits_k n_0^{ijk} p_i(H_{1/3}, T_z) p_j(\beta) p_k(U) F_0^{ijk}(x)}{\sum\limits_i \sum\limits_j \sum\limits_k n_0^{ijk} p_i(H_{1/3}, T_z) p_j(\beta) p_k(U)} \tag{21}$$

where $p_i(H_{1/3}, T_z)$, $p_j(\beta)$ and $p_k(U)$ are the probability of each wave state, wave heading angle and navigational speed, respectively; $f_0{}^{ijk}(x)$ and $F_0{}^{ijk}(x)$ are the probability density function and cumulative distribution function for each specified short-term condition, respectively; $n_0{}^{ijk}$ is the cycle times of alternate loads within unit time period and it differs for each short-term condition, and it is obtained by:

$$n_0^{ijk} = \frac{n_{ijk}}{T_{ijk}} \tag{22}$$

where n_{ijk} is the cycle number of motion or load signal within the whole simulation time T_{ijk}.

The probability that the peak value exceed a specified value x_a can be obtained by:

$$P\{X \geq x_a\} = \int_{x_a}^{\infty} f(x)\mathrm{d}x = 1 - F(x_a) = \frac{1}{n} \tag{23}$$

where the probability of exceedance P is the reciprocal of the cycle number n, i.e., the number of waves encountered of a ship during the return period. The value of n is usually set at 10^8 for determination of the long-term design loads.

3. Experimental Validation of the Hydroelasticity Theory

3.1. Experimental Setup

A 1/50 scaled segmented model was designed and built according to the full-scale ship. The main dimensions of the ship and the model are listed in Table 1. The model is divided into seven parts longitudinally and cuts are provided at stations number 2, 4, 6, 8, 10 and 12. Steel backbones with variational cross-section are used to connect the segments and sectional loads on the backbone are measured at the six cut sections. The backbones are designed according to the principle of stiffness similarity. A self-propelling mechanical system is designed at the stern region of the model to achieve the expected speed of the ship in waves.

Table 1. Main dimension of the ship.

Item	Symbol	Full Scale	Small Model
Scale	λ	1:1	1:50
Overall length (m)	L_{OA}	312	6.24
Waterline length (m)	L	292	5.84
Moulded breadth (m)	B	39.5	0.79
Depth (m)	D	25.5	0.51
Draft (m)	T	10.1	0.202
Block coefficient	C_B	0.616	0.616
Displacement (t)	Δ	71,875	0.575

The tests were conducted in the ship model towing tank of Harbin Engineering University, which has a dimension of 108 m long by 7 m wide by 3.5 m deep. A towing carriage that travels along the tank is used to serve as the platform of translational movement system. A computerized flat-type wave generator that can generate both regular and irregular waves is located at the end side of tank. The incident waves will be absorbed by a damping beach located at the other side of tank to prevent wave reflection. A wave probe is positioned near the wave generator to monitor and record the generated waves. Wave-induced ship motions are measured by an in-house developed, four-DOF contact-type seakeeping apparatus, which is installed on the towing carriage and connected to the ship model by its two heave sticks. The ship model and tank facilities are shown in Figure 3.

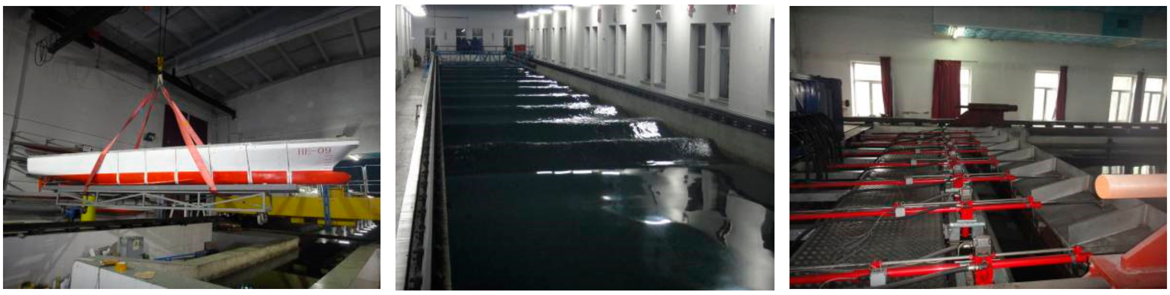

(**a**) (**b**) (**c**)

Figure 3. Model and tank facilities. (**a**) Model overview; (**b**) wave tank; (**c**) wave-maker.

3.2. Numerical Setup

A corresponding full-scale numerical model is established and the hydroelastic responses are calculated by the developed hydrodynamic code. The established whole ship hydrodynamic grid and the wetted grid under waterline are shown in Figure 4. The whole ship hydrodynamic grid which includes 2055 panels is used for the Froude–Krylov force and hydrostatic restoring force calculation; the underwater wetted grid, which includes 1308 panels, is used for diffraction force and radiation force calculation. In addition, the hull structure is discrete by 20 Timoshenko beam elements and the vertical vibration mode of the hull girder in vacuum is solved by the transfer matrix method (TMM).

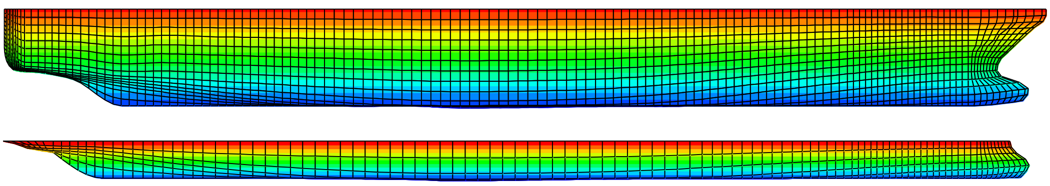

Figure 4. Hydrodynamic calculation grid.

Two experimental conditions are selected for comparison with the numerical results: the extreme sea state Condition 1 ($H_{1/3}$ = 15 m, T_z = 12.25 s, U = 5 knots) and the high speed Condition 2 ($H_{1/3}$ = 9.2 m, T_z = 11.4 s, U = 24 knots). The long-crested irregular waves are generated using ISSC target spectra. The ship short-term responses within 1 h are simulated by the numerical hydroelastic code. Enough experimental time and samples are achieved by combining the time series at steady run region measured in several different runs.

3.3. Comparison of Numerical and Experimental Time Series

The comparison of numerical and experimental time series of full-scale ship vertical motion and loads in the selected Condition 1 ($H_{1/3}$ = 15 m, T_z = 12.25 s, U = 5 knots) and Condition 2 ($H_{1/3}$ = 9.2 m, T_z = 11.4 s, U = 24 knots) are shown in Figures 5 and 6, respectively. It is noted that the total VBM amidships were separated into low-frequency (LF) wave loads and high-frequency (HF) whipping loads by Fourier filter. As seen from the comparison, it is clear that the curves show similar trends and magnitudes between numerical simulation and experimental measurement results. It should be noted that the numerical and experimental time series will not agree in detail since the exact elevation of incident waves acting on the model was not measured during the experiment. Only an in situ wave probe that located in front of the wave maker was used to measure the experimental waves. Therefore, the numerical irregular waves are generated by using the random initial phase.

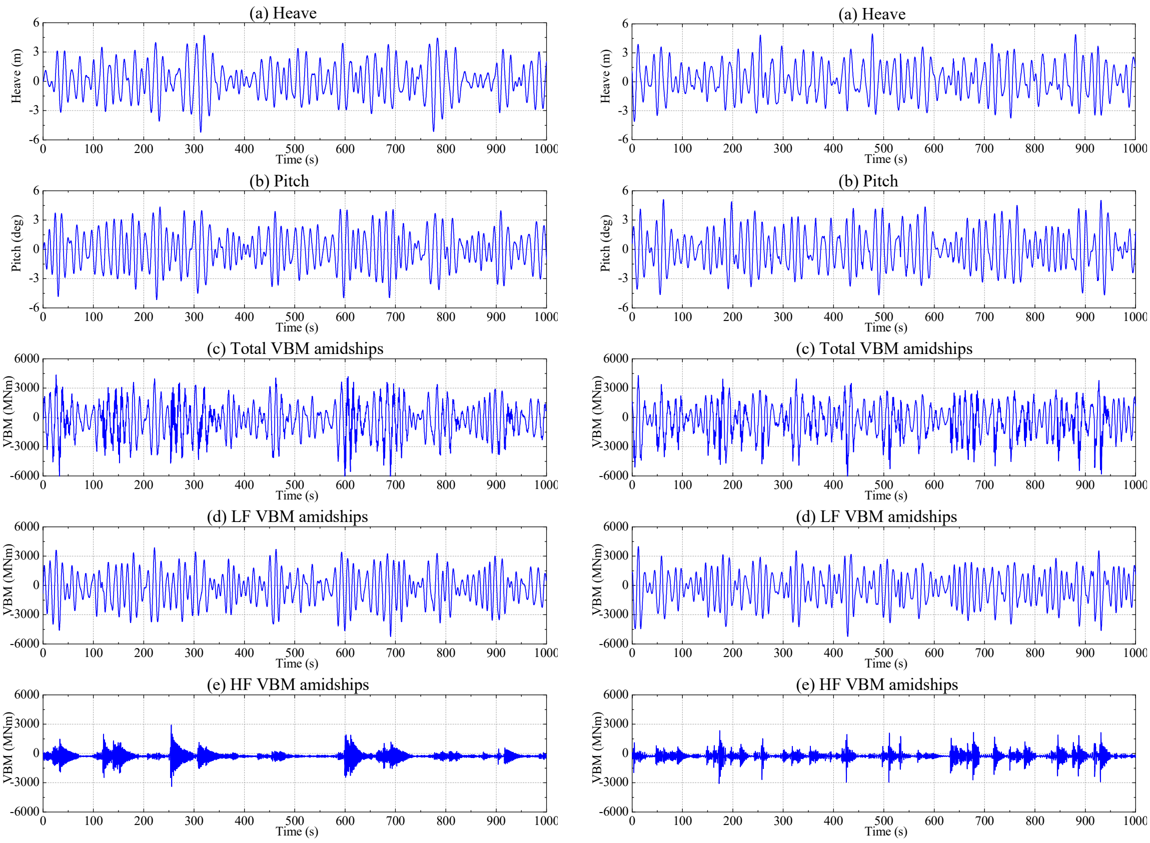

Figure 5. Time series of motion and loads in Condition 1. (**left**) Numerical results; (**right**) experimental results.

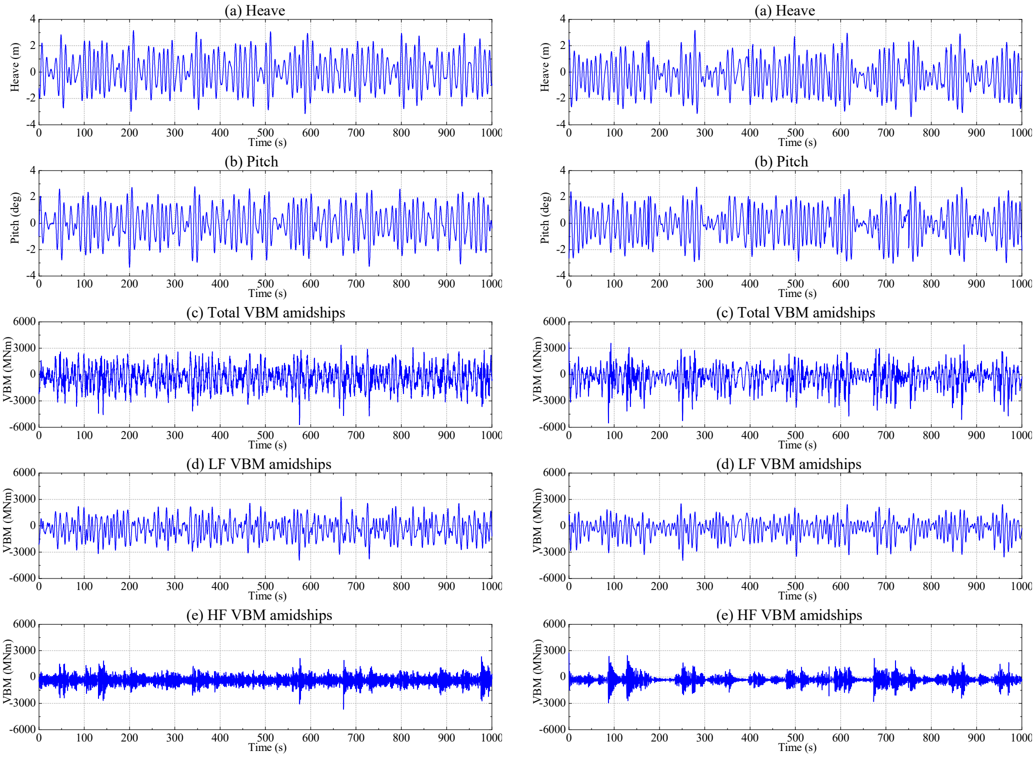

Figure 6. Time series of motion and loads in Condition 2. (**left**) Numerical results; (**right**) experimental results.

3.4. Comparison of Numerical and Experimental Spectra

The frequency response spectra are usually used to describe the ship short-term responses in irregular waves. Comparisons of the frequency spectral results of ship heave, pitch and VBM amidships in the two afore-mentioned conditions are shown in Figures 7–9. The spectra are obtained by the auto-correlation function method with Hamming smooth processing based on the corresponding time series. As can be seen, the frequency distribution and peak value of the response spectra show good agreement between the numerical and experimental results in both the two conditions. The peak frequency of heave, pitch and VBM spectra increases from Condition 1 to Condition 2 due to the increasing wave encounter frequency. However, the fill area under the curve, which denotes variance decreases from Condition 1 to Condition 2 due to the decreasing wave state. The spectral density concentrates within the narrow range of 0.3~0.8 rad/s for heave and pitch motions. However, to be different from the motion spectra, the VBM spectra comprise both low frequency and high frequency components, which is consistent with the phenomena observed from the time histories in Figures 5 and 6. The frequency of whipping loads coincides with the two-node wetted natural frequency of the hull. Moreover, the slamming loads are more pronounced at the high-speed condition.

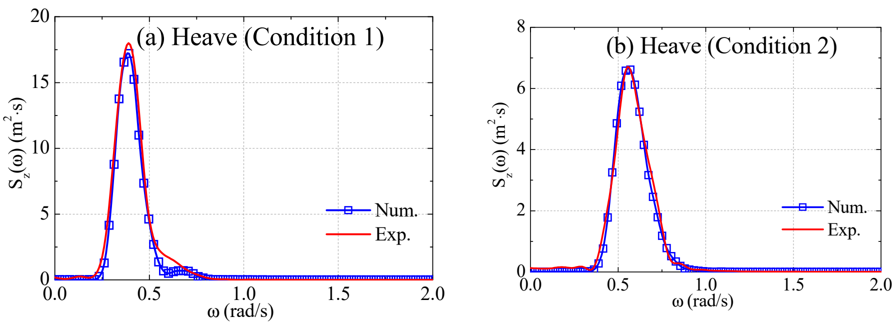

Figure 7. Comparison of heave spectra.

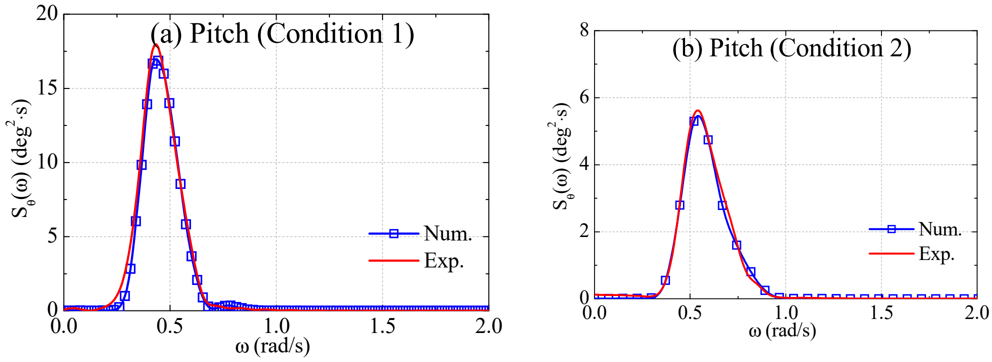

Figure 8. Comparison of heave spectra.

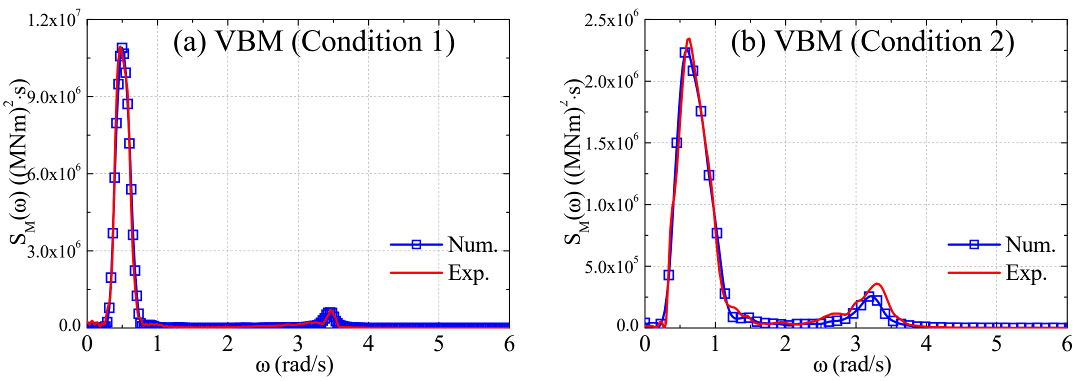

Figure 9. Comparison of heave spectra.

3.5. *Probability of Exceedance of Numerical and Experimental Peaks*

The peak values, including both crest and trough, are counted in each zero-up-crossing period of the time series for heave and pitch motions. The comparison between numerical and experimental probability of exceedance of heave and pitch peaks in the two wave conditions are shown in Figures 10 and 11, where good agreement is achieved between the numerical and experimental results. However, the asymmetry distribution of crest and trough values is more pronounced for the experimental results than the numerical results since the numerical method do not include any steady effects due to forward speed. The numerical extreme values of heave and pitch motions are generally larger than the experimental values.

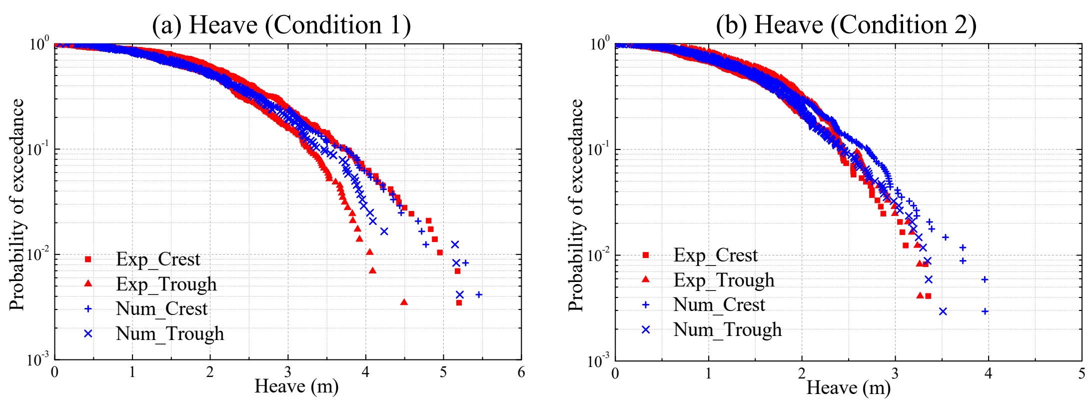

Figure 10. Comparison of probability of exceedance of heave motion.

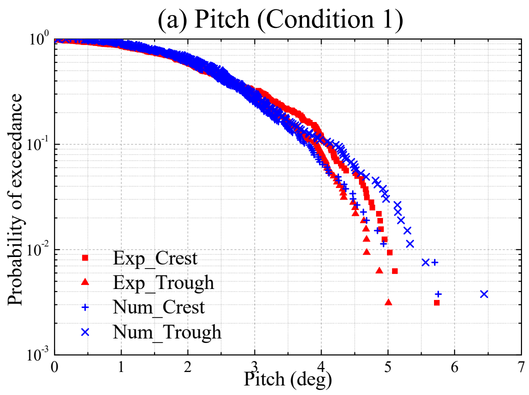

Figure 11. Comparison of probability of exceedance of pitch motion.

In addition, it is of great importance to investigate the asymmetric behavior of VBM in hogging and sagging especially in severe waves. The comparison of numerical and experimental probability of exceedance of VBM amidships (includes both total VBM and LF VBM) is shown in Figure 12. As is seen, both the numerical and experimental results reveal a highly asymmetrical distribution in hogging and sagging peaks, and the sagging VBM is much larger than hogging VBM. The difference between numerical and experimental results is obvious especially for the high-speed condition. One probable reason is that the Froude–Krylov weakly nonlinear hydroelastic code cannot fully reproduce the strongly nonlinear load characteristic of bow flare ship in harsh irregular waves. Another reason may be that the momentum impact theory for HF slamming loads estimation ignores the water pile up effects and water exit force. In the future, more complex and accurate hydroelastic algorithm will be developed and compared with the experimental results.

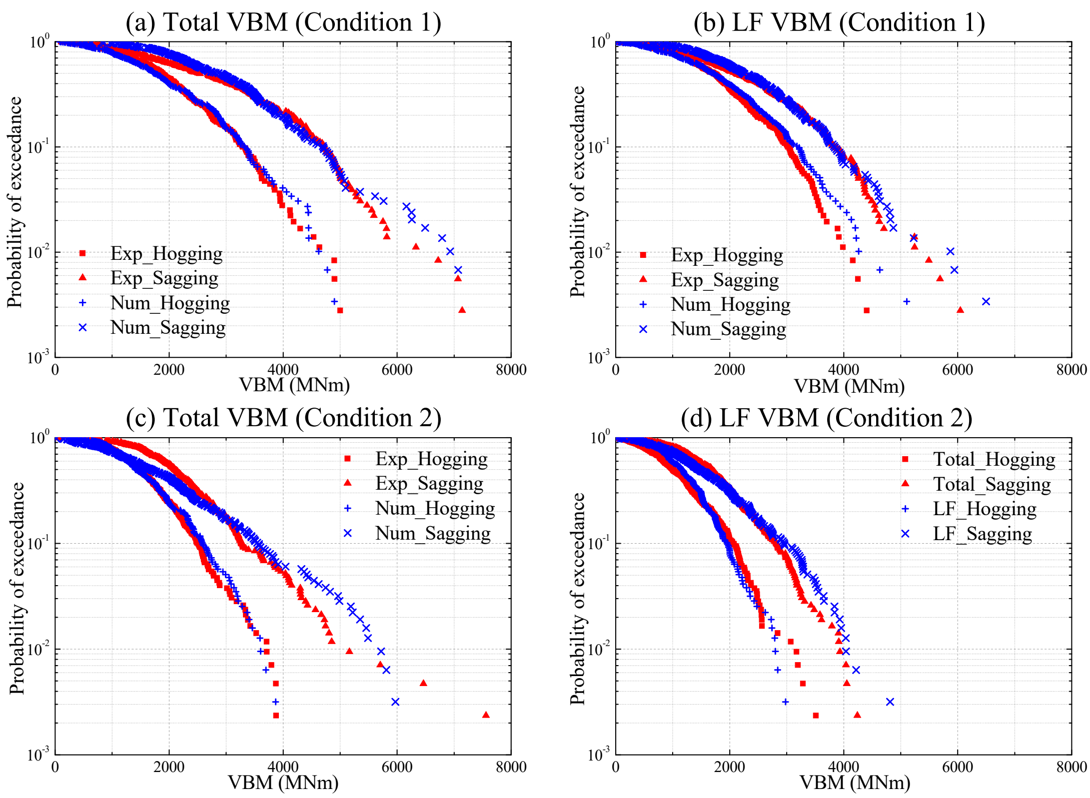

Figure 12. Probability of exceedance of total VBM peaks.

4. Statistical Analyses of Numerical Simulation Results

4.1. Calculation Method and Procedure

The time series of short-term motion and load responses under specified wave state, navigational speed, wave heading and loading condition can be calculated using the developed time-domain hydroelastic code. The crest and trough peak values in each zero-up-crossing period are counted and then they are used to derive the statistical values such as single significant amplitude or root mean square. Moreover, the Weibull distribution function is used to fit the probability density distribution of the peaks obtained in each short-term period.

An example of the short-term statistical analysis using the numerical data of VBM amidships in Condition 2 is shown as follows. Figure 13 presents the simulated time series of VBM within 1 h and the 100 s local view from 1200 s to 1300 s with explanation of the statistical values. It is noted that the short-term predictions are conducted respectively by adopting the nonlinear hydroelasticity theory considering slamming loads and the linear hydroelasticity theory without considering slamming loads. Figure 14 presents the corresponding histogram of the statistical hogging and sagging VBM peak values as well as the Weibull fitting results. In addition, Figures 15 and 16 present the histogram of the statistical crest and trough values of heave and pitch motions as well as the Weibull fitting results. It is noted that the presented motion results are obtained by nonlinear hydroelastic numerical simulation and the motion signals are turned out to be associated with less nonlinearity compared with the loads. The distributions of heave and pitch peaks are close to Rayleigh distribution, which is a kind of special Weibull distribution.

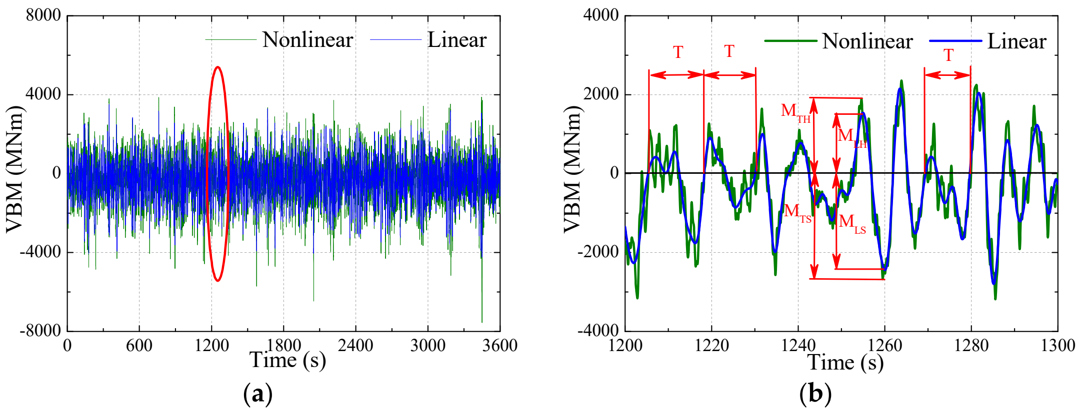

Figure 13. Statistics of peak values from the short-term simulation results. (**a**) The simulated time series in 1 h; (**b**) zoom view of time series in 100 s.

The long-term motion and load responses under a series of different wave states, navigational speeds, wave headings and loading conditions can be predicted based on the short-term prediction results according to the method described in Section 2.3. Moreover, in order to identify the influence of whipping loads on hull girder ultimate strength, the long-term extreme loads that obtained by nonlinear hydroelasticity theory and linear hydroelasticity theory are compared and the ratio coefficient of extreme loads is used to describe the influence of whipping loads on total loads. The ratio coefficient is also used for subsequent hull girder ultimate strength assessment in combination with classification society Rules approach. The flowchart of the long-term prediction of extreme loads and subsequent structural ultimate strength assessment is summarized in Figure 17.

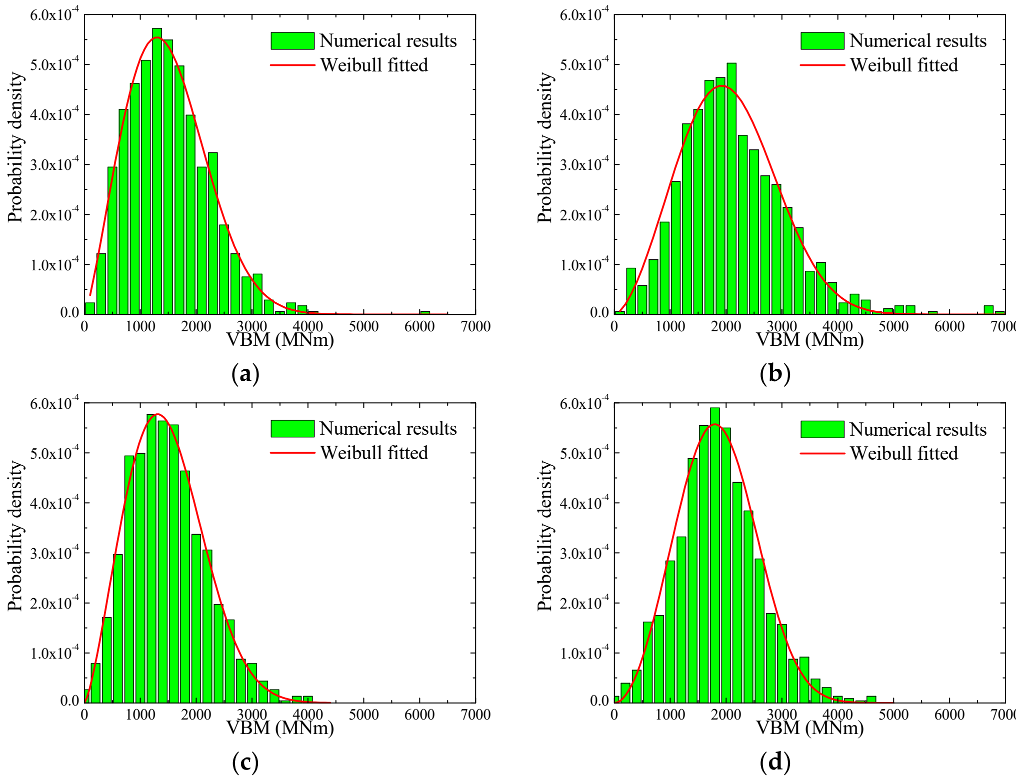

Figure 14. The histogram of VBM peak distribution. (**a**) Nonlinear hogging VBM; (**b**) nonlinear sagging VBM; (**c**) linear hogging VBM; (**d**) linear sagging VBM.

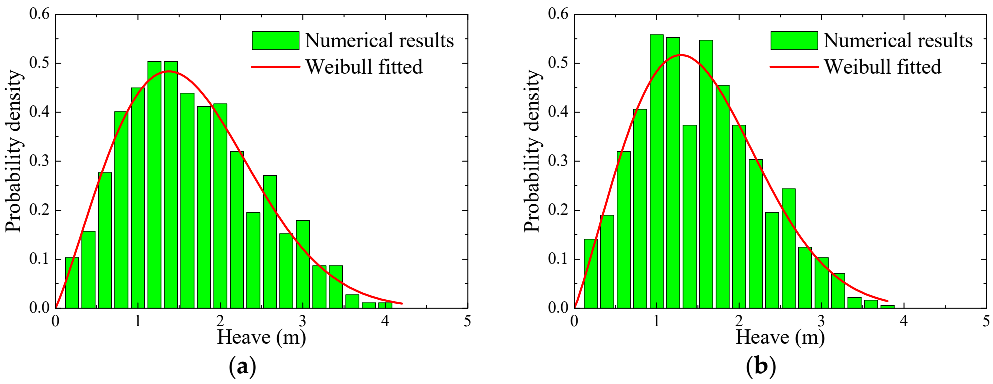

Figure 15. The histogram of heave peak distribution. (**a**) Nonlinear heave crest; (**b**) nonlinear heave trough.

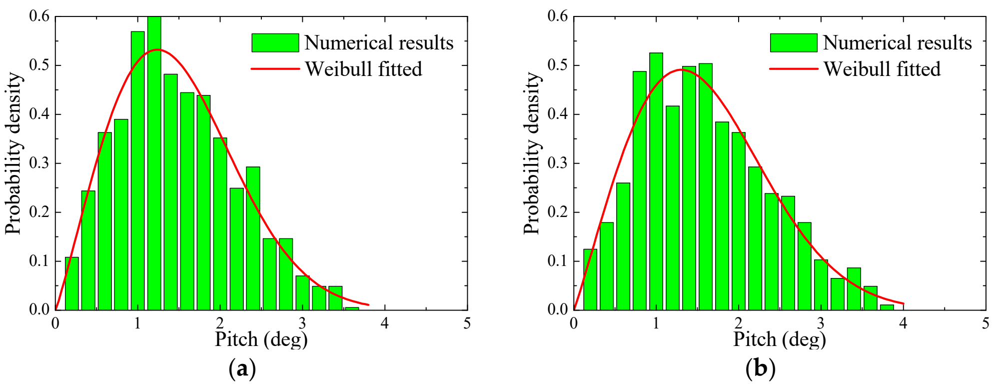

Figure 16. The histogram of pitch peak distribution. (**a**) Nonlinear pitch crest; (**b**) nonlinear pitch trough.

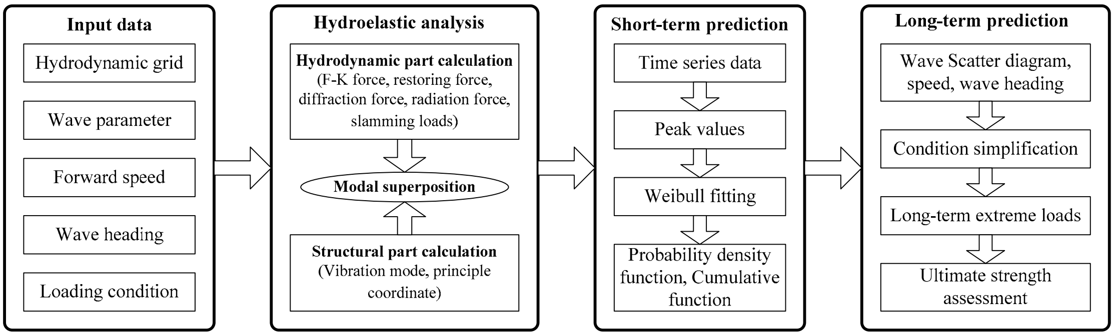

Figure 17. Flowchart of the wave loads prediction and ultimate strength assessment.

4.2. Simplification of Calculation Conditions for Long-Term Prediction

Since the 3D time-domain nonlinear numerical simulation is a time-consuming process, it is desirable to carry out as few simulations as possible. The contribution of short-term loads to the long-term extreme loads differs significantly for different short-term conditions. It has been turned out that the long-term extreme value estimated by using results with limited number of short-term condition is reasonable and the difference between the predicted extreme values is ignorable small within 1%. The simplification scheme of numerical simulation conditions is discussed and analyzed as follows.

We assume the incident waves to be long-crested in this calculation. The fundamental work for long-term prediction is to select appropriate wave environments in which the ship will operate during its lifetime. Wave environment in long-term is usually described by wave scatter diagrams and the North Atlantic open sea states are chosen in this study. As seen from Table 2, the number of combinations of significant wave heights and characteristic periods is 197. In addition, the wave heading angles ranging from 0° to 180° are divided into 7 representative values with the same interval of 30°. The probabilities of heading angles 0°, 30°, 60°, 90°, 120°, 150° and 180° are set as 1/12, 1/6, 1/6, 1/6, 1/6, 1/6, and 1/12, respectively. So there are 1379 short-term wave environment states in total, which could be very large. In fact, whipping is most pronounced in head or near head waves at high seas and the extreme load usually occurs in severe head or bow oblique waves. For simplification, only 44 wave conditions that with significant wave height higher than 12 m are involved in the long-term prediction. In addition, only head wave 0° and bow oblique wave 30° and 60° are involved in the long-term prediction.

Ship motions and wave loads depend not only on sea states and wave heading angles but also on the forward speed among other things. The influence of ship forward speed on wave loads could be obvious since the whipping loads are sensitive to the change of speed. In fact, the ship forward speed can be involuntary reduced because of added resistance in waves. In addition, in severe sea states the ship's master usually reduces the speed in order to avoid excessive ship motions, accelerations, slamming and green water on deck. In this study, the selected speeds in relation with the significant wave heights are listed in Table 3, where *Vs* is the design service speed and it is selected as 24 knots in this study. Moreover, the influence of loading condition on the extreme value in long-term prediction is not considered since the involved ship in this study is a warship and her weight distribution change is small.

Table 2. Scatter diagram for the North Atlantic sea states.

Hs/Tz	**1.5**	**2.5**	**3.5**	**4.5**	**5.5**	**6.5**	**7.5**	**8.5**	**9.5**	**10.5**	**11.5**	**12.5**	**13.5**	**14.5**	**15.5**	**16.5**	**17.5**	**18.5**	**Sum**
0.5			1.3	133	865	1186	634	186	36.9	5.6	0.7	0.1							**3050**
1.5				29.3	986	4976	7738	5569	2375	703	160	30.5	5.1	0.8	0.1				**22,575**
2.5				2.2	197	2158	6230	7449	4860	2066	644	160	33.7	6.3	1.1	0.2			**23,810**
3.5				0.2	34.9	695	3226	5675	5099	2838	1114	377	84.3	18.2	3.5	0.6	0.1		**19,128**
4.5					6	196	1354	3288	3857	2685	1275	455	130	31.9	6.9	1.3	0.2		**13,289**
5.5					1	51	498	1602	2372	2008	1126	463	150	41	9.7	2.1	0.4	0.1	**8328**
6.5					0.2	12.6	167	690	1257	1268	825	386	140	42.2	10.9	2.5	0.5	0.1	**4806**
7.5						3	52.1	270	594	703	524	276	111	36.7	10.2	2.5	0.6	0.1	**2586**
8.5						0.7	15.4	97.9	255	350	296	174	77.6	27.7	8.4	2.2	0.5	0.1	1309
9.5						0.2	4.3	33.2	101	159	152	99.2	48.3	18.7	6.1	1.7	0.4	0.1	**626**
10.5							1.2	10.7	37.9	67.5	71.7	51.5	27.3	11.4	4	1.2	0.3	0.1	**285**
11.5							0.3	3.3	13.3	26.6	31.4	24.7	14.2	6.4	2.4	0.7	0.2	0.1	**124**
12.5							0.1	1	4.4	9.9	12.8	11	6.8	3.3	1.3	0.4	0.1		**51**
13.5								0.3	1.4	3.5	5	4.6	3.1	1.6	0.7	0.2	0.1		**21**
14.5								0.1	0.4	1.2	1.8	1.8	1.3	0.7	0.3	0.1			**8**
15.5									0.1	0.4	0.6	0.7	0.5	0.3	0.1	0.1			**3**
16.5										0.1	0.2	0.2	0.2	0.1	0.1				**1**
Sum	**0**	**0**	**1**	**165**	**2091**	**9280**	**19,922**	**24,879**	**20,870**	**12,898**	**6245**	**2479**	**837**	**247**	**66**	**16**	**3**	**1**	**100,000**

Percentage
- 0–100
- 100–500
- 500–1000
- 1000–2000
- 2000–3000
- 3000–5000
- 5000–7000
- 7000-

Table 3. The calculation speed at different significant wave heights.

$H_{1/3}$ (m)	U (knot)
$0 < H_{1/3} \leq 6$	Vs
$6 < H_{1/3} \leq 9$	75%Vs
$9 < H_{1/3} \leq 12$	50%Vs
$12 < H_{1/3}$	25%Vs ($\geq$5)

4.3. Short-Term Response Analyses

The short-term statistical values of motion and load responses in the typical numerical simulation Conditions 3~9 ($H_{1/3}$ = 12 m, T_z = 13.5 s, U = 24 knots, β = 0, 30°, 60°, 90°, 120°, 150° and 180°) are analyzed in this section. It is noted that the wave characteristic period is determined according to the principle that the ratio of the average wave length to the ship length is close to 1. The simulations were made by using both linear and nonlinear hydroelastic theory and same incident wave time series were provided for the two schemes for the sake of consistency. Figure 18 shows the comparison of mean value of crest and trough peaks of heave, pitch and total VBM amidships that counted based on the numerical time series. As can be seen from the results, the largest heave and pitch motions occurred at bow oblique waves 30° or 60°, which can be explained by the relationship between encountered frequency and resonant frequency. The heave and pitch peaks that obtained by nonlinear hydroelastic theory are generally smaller than those by linear hydroelastic theory since the local slamming force (or moment) are always opposite the ship heave (or pitch) direction it could buffer the motion amplitude. The VBM amidships for a ship sailing in head or bow oblique waves that predicted by nonlinear hydroelastic theory are much larger than those by linear theory due to the occurrence of whipping loads. The smallest VBM values occurred when a ship sails in beam waves.

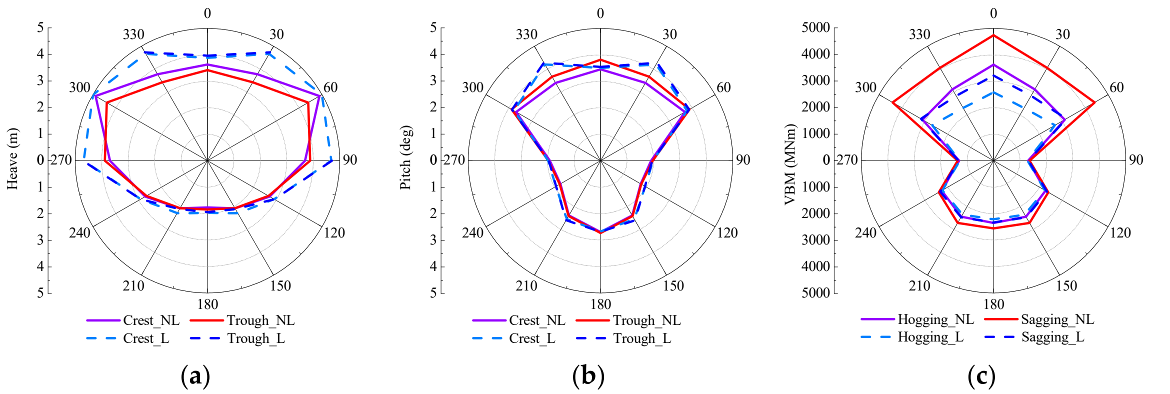

Figure 18. Comparison of short-term extreme values between linear and nonlinear schemes. (**a**) Heave; (**b**) pitch; (**c**) VBM.

In addition, the time series of VBM amidships in the wave condition ($H_{1/3}$ = 12 m, T_z = 13.5 s, U = 24 knots) while sailing at different wave headings are summarized in Figure 19. The total VBM were separated into LF wave loads and HF whipping loads with a cut-off frequency of 0.3 Hz. As is seen, frequent and severe slamming events occurred when the ship sailing in head waves. The magnitude of whipping loads is even larger than the wave loads, which results in the occurrence of extreme large total sagging loads. Significant whipping loads are also observed for a ship sailing in bow oblique waves 30° and 60° even though they are not as severe as those for head waves. The whipping loads are very weak when ship sailing in beam waves and the whipping loads are almost disappeared when ship sailing in stern oblique waves 120° mainly due to the relatively low encountered frequency. However, moderate whipping loads are found again for a ship sailing in stern oblique waves 150° and following waves.

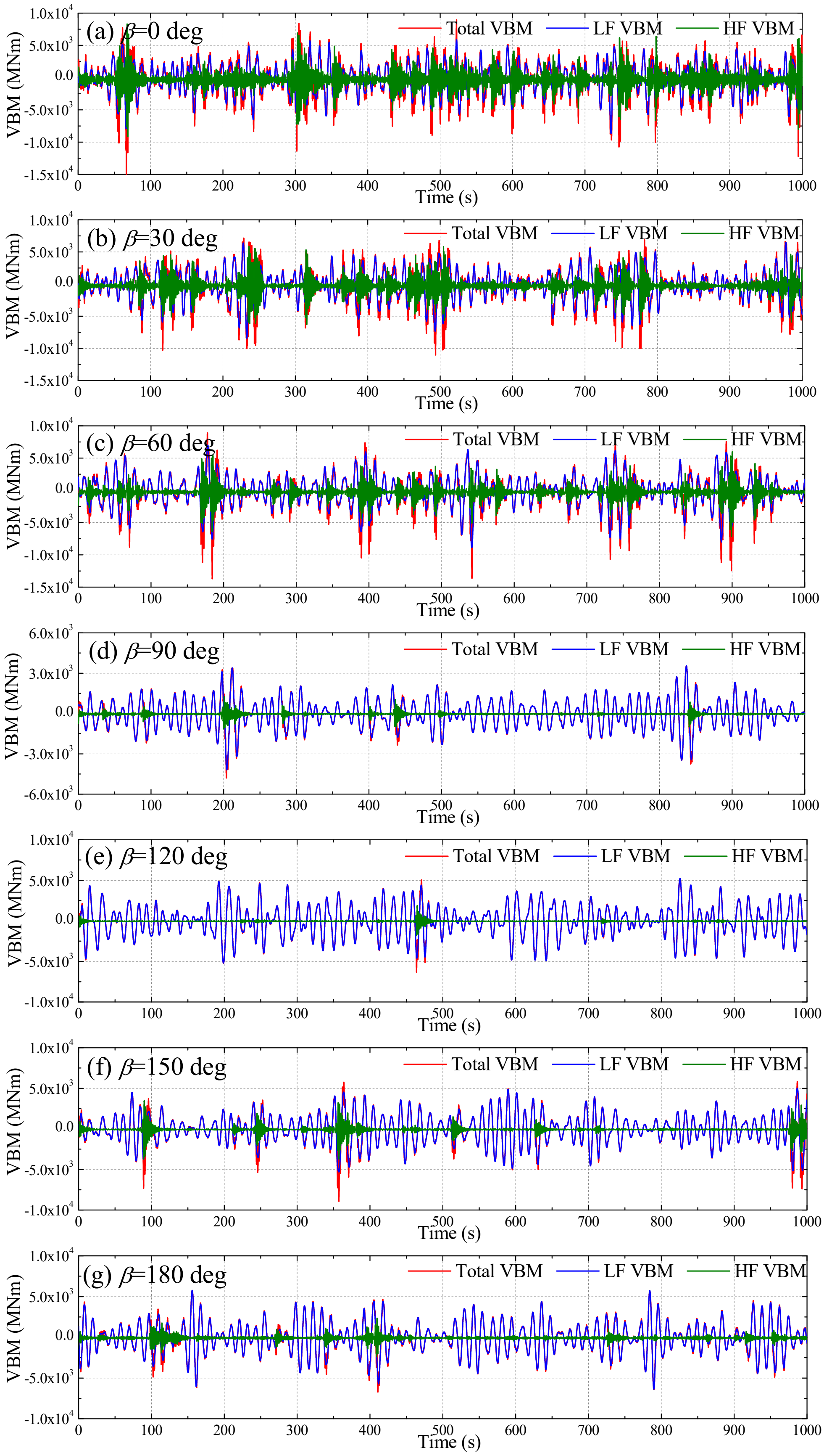

Figure 19. VBM load components in different wave headings.

4.4. Long-Term Extreme Loads

The long-term prediction results of VBM amidships under different probability levels 10^{-1}~10^{-9} obtained by both linear and nonlinear hydroelastic theory are compared in Figure 20. The results indicate that the linear hydroelastic theory underestimates the extreme load by approximately 10% compared with the nonlinear results. The nonlinear sagging VBM extreme values are obviously larger than the hogging values due to the whipping effects. In addition, in order to investigate the influence of condition simplification on the long-term prediction results, Table 4 lists the long-term prediction results under probability level 10^{-8} that obtained by nonlinear hydroelasticity theory using both the full simulation conditions and the simplified short-term conditions (132 conditions in total, i.e., 44 wave conditions by three heading angles). The results indicate that the difference between the predicted extreme values by the two simulations is ignorable small within 1%.

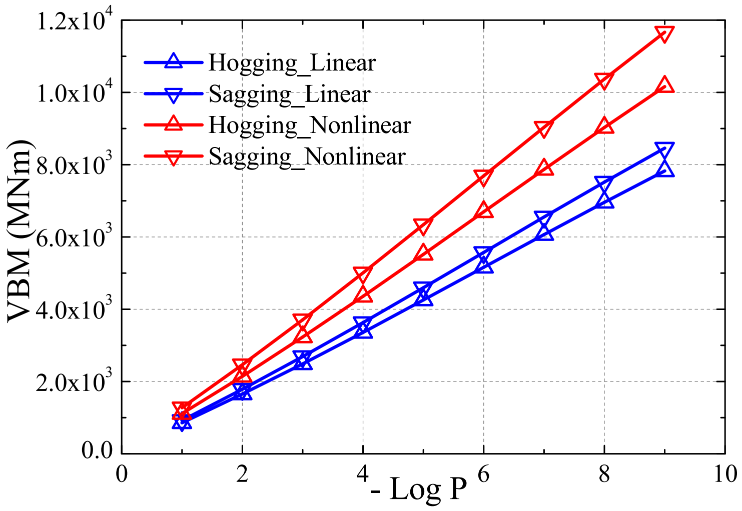

Figure 20. Long-term prediction results of VBM amidships.

Table 4. Extreme of VBM amidships at probability level 10^{-8}.

Item		Full Conditions	Simplified Conditions	Error
Nonlinear results (MNm)	Hogging	9036	9030	0.07%
	Sagging	10382	10370	0.12%
Linear results (MNm)	Hogging	6971	6959	0.17%
	Sagging	7533	7516	0.23%
Ratio coefficient	Hogging	1.296	1.298	0.15%
	Sagging	1.378	1.380	0.15%

5. Hull Girder Ultimate Strength Assessment

5.1. The Proposed Strength Check Formula

The evaluation of structural strength is of great importance in the design of ships especially for a naval ship operating in harsh weather. Fundamental to the hull structural strength assessment is the accurately prediction of extreme design loads to support the Rule requirements and for application in direct calculations. In fact, the contribution of whipping loads to extreme design loads is not carefully considered in majority of the present classification society Rule approaches. With this in mind, an improved Rule approach is proposed to evaluate the ultimate strength of hull structure based on the long-term extreme value results of ship wave loads and slamming loads by direct calculation:

$$\gamma_S M_S + \gamma_W f_{whip} M_W \leq \frac{M_U}{\gamma_R \gamma_M} \tag{24}$$

where M_S, M_W and M_U are calm water VBM, wave-induced VBM and ultimate VBM capacity of hull transverse section, respectively; γ_S, γ_W, γ_R and γ_M are the safety factor due to uncertainty of M_S, M_W, M_U and material, respectively; f_{whip} is correction factor of wave load due to whipping loads and is obtained as follows:

$$f_{whip} = C_{un} \frac{M_{whip}}{M_{wave}} \tag{25}$$

where C_{un} is the safety factor due to simplification of calculation conditions, M_{whip} is the extreme value load of hogging or sagging VBM that estimated by direct calculation using nonlinear hydroelasticity theory considering slamming loads, M_{wave} is the extreme value load of hogging or sagging VBM estimated by direct calculation using linear hydroelasticity theory without considering slamming loads.

5.2. Determination of Design Loads by Rule Approach

In this study, the Rules for the Classification of Military Ships [33] issued by Bureau Veritas (BV) is used as an example to determine the design wave loads. According to Rules Book, the still water VBM amidships in hogging or sagging conditions, in MNm, can be obtained by:

$$M_S^H = 175 \times 10^{-6} F_S C L^2 B (C_B + 0.7) - M_W^H \tag{26}$$

$$M_S^S = 175 \times 10^{-6} F_S C L^2 B (C_B + 0.7) + M_W^S \tag{27}$$

where

- F_S denotes distribution factor defined as follows: 0.2 at FP and AP points, 1 between 0.3 and 0.7 L, and liner interpolation at other intervals,
- C denotes wave coefficient calculated by $C = 10.75 - (300 - L/100)^{1.5}$ for ships with a waterline length L between 90 and 300 m,
- L denotes ship waterline length, B denotes moulded breadth, C_B denotes block coefficient,
- ${M_W}^H$ and ${M_W}^S$ denotes wave-induced VBM amidships in hogging and sagging, respectively. They are obtained as follows.

The vertical wave-induced bending moments at any section are obtained by:

$$M_W^H = 150 \times 10^{-6} F_M C L^2 B C_B (1 + C_A) \tag{28}$$

$$M_W^S = -85 \times 10^{-6} F_M C L^2 B (C_B + 0.7)(1 + C_A) \tag{29}$$

where

- F_M denotes distribution factor defined as follows: 0 at FP and AP points, 1 between 0.4 and 0.65 L, and liner interpolation at other intervals,
- C_A is coefficient obtained by $C_A = 7.1 H_A(1 + 1.26F)/L$, where F denotes ship length Froude's number,
- H_A denotes wave parameter $H_A = CL/200$ and without being taken greater than $0.8C$.

The calculated distribution of still water VBM and wave induced VBM along ship length by the above-mentioned equations are shown in Figure 21.

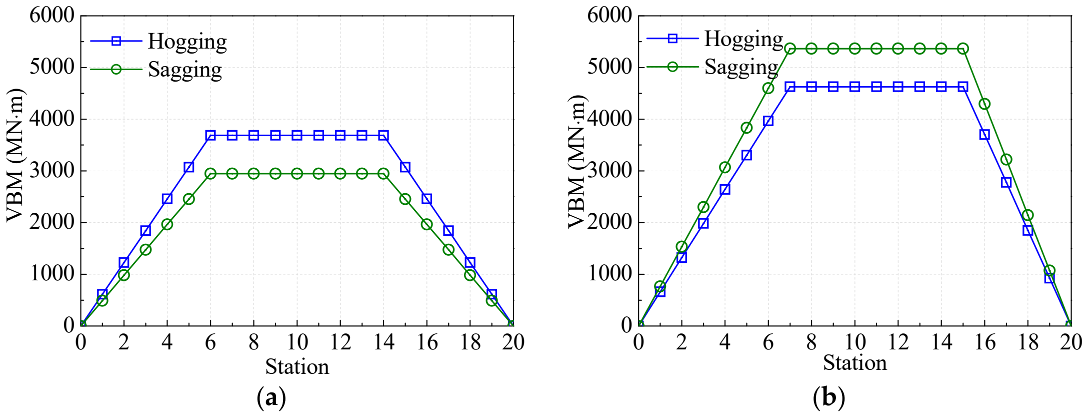

Figure 21. Distribution of design loads of VBM. (**a**) Still water VBM; (**b**) wave-induced VBM.

5.3. Ultimate Bearing Capacity Assessment

The hull transverse section amidships is adopted for ultimate strength assessment in this study. Figure 22 shows the structural finite element model of the selected calculation transverse section. The ultimate bending moment capacities for hogging and sagging VBM are determined by the maximum and minimum values of the curve of bending moment capacity M versus the curvature χ of the transverse section amidships. The curve M-χ shown in Figure 23 is obtained by incremental-iterative approach (the so-called Smith's simplified method). During the calculation procedure, the incremental procedure is represented by the calculation of the bending moment M_i, which acts on the hull transverse section as the effect of an imposed curvature χ_i. For each step, the value χ_i is obtained by summing an increment of curvature $\Delta\chi$ to the value relevant to the previous step χ_{i-1}. This rotation increment induces axial strains ε in each hull structural element depends on the position of the element. The stress σ induced in each structural element by the strain ε is obtained from the load-end shortening curve σ-ε of the element. The position of neutral axis is calculated and updated at each iterative step. Once the stress distribution in the section structural elements is obtained, the bending moment M_i around the new neutral axis can be obtained by summing the contribution given by each element stress.

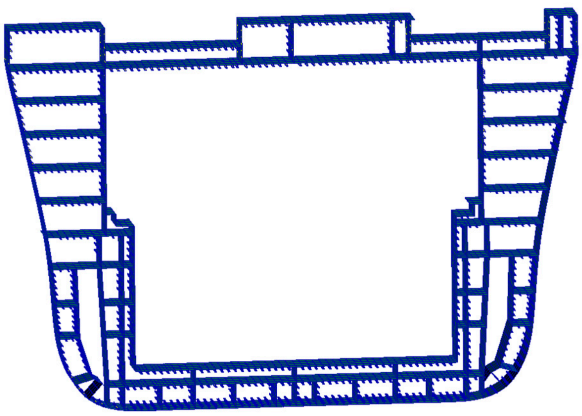

Figure 22. Structural finite element model of the calculation section.

The results of the determined design loads and ultimate bearing capacity in hogging and sagging conditions are summarized in Table 5. The safety factors are determined as per the Rule Book. The overall VBM loads by the Rule approach is obtained using the calm water VBM and wave-induced VBM and their safety factors (i.e., the left-hand side of Equation [24]), the overall VBM loads by direct calculation are the long-term prediction values by nonlinear hydroelasticity theory considering whipping loads. The results indicate that the extreme design hogging and sagging VBM loads by Rule approach are 12.3% and 6.4% larger than the values by nonlinear hydroelastic direct calculation, respectively. The ultimate bearing capacity of hull section is compared with the extreme design loads that determined by both the Rule approach and the direct calculations. To summarize, the hull section structural strength satisfies the safety requirement that checked by both of the two methods.

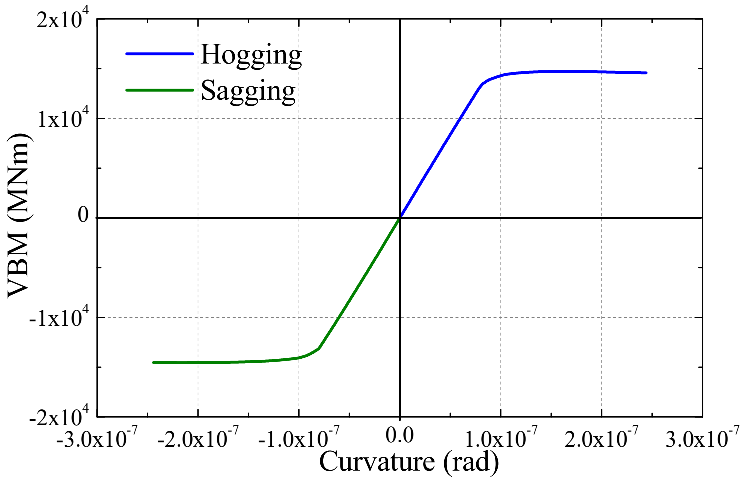

Figure 23. The calculated curve of VBM versus curvature.

Table 5. Hull girder ultimate strength assessment results.

Item	Symbol	Hoging	Saging
Calm water VBM	M_S (MNm)	3688	2948
Wave-induced VBM	M_W (MNm)	4627	5366
Extreme VBM by nonlinear direct calculation	M_{whip} (MNm)	9036	10,382
Extreme VBM by linear direct calculation	M_{wave} (MNm)	6971	7533
Correction factor due to whipping loads	f_{whip}	1.30	1.38
Safety factor of M_S	γ_S	1.00	1.00
Safety factor of M_W	γ_W	1.10	1.10
Safety factor of M_U	γ_R	1.15	1.15
Safety factor of material uncertainty	γ_M	1.02	1.02
Safety factor of condition simplification	C_{un}	1.01	1.01
Ultimate bearing capacity VBM	M_U (MNm)	14,713	14,550
Strength check by Rule approach	M_{Total} (MNm)	10,305	11,094
	Failure ratio	82%	88%
	Safety satisfy?	Yes	Yes
Strength check by direct calculation	M_{Total} (MNm)	9036	10,382
	Failure ratio	72%	83%
	Safety satisfy?	Yes	Yes

6. Conclusions

In this paper, a time-domain hydroelastic method for wave-induced ship nonlinear motions and loads prediction is presented. The hull girder is modeled as a 1D flexible beam so that the hydroelastic responses and slamming induced whipping responses are properly considered. Then a nonlinear long-term statistics method in terms of the probability of exceedance and extreme value is presented based on the time-domain nonlinear short-term simulation results. The calculated long-term vertical sagging and hogging moments amidships are further used to provide classification society Rules for ultimate strength assessment. The following conclusions can be obtained from this study:

(1) The developed time-domain hydroelastic theory, which combines 3D BEM and 1D beam model is reliable in the prediction of ship nonlinear motion and load responses and it has been well

validated by comparison with the tank experimental results. Since the developed hydroelastic code runs much faster than the more complicated algorithm, which combines 3D BEM and 3D FEM, it is applicable for direct calculation of extreme wave loads and other nonlinear responses by performing long time numerical simulation.

(2) The slamming induced whipping loads acting on ship when sailing in harsh waves and at high speed significantly increase the extreme loads for head or bow oblique wave conditions, while the whipping loads are very weak when ship sailing in beam or stern oblique waves. The long-term extreme VBM load predicted by nonlinear hydroelastic theory considering slamming effects is approximately 30% higher than that by linear hydroelastic theory. The simplification of simulation condition has ignorable small influence on the long-term extreme values.

(3) Due to the fact that the effects of whipping loads on a hull girder's ultimate strength is not well considered in the majority of the present Rule Book approaches, a simplified strength check formula, which includes the whipping load coefficient, is developed on the basis of the design wave loads by classification society Rule approach. The developed strength check formula is very useful for the hull girder ultimate strength assessment of a large flexible ship with a flare bow operating in harsh conditions.

Author Contributions: J.J. and Y.J. conducted the numerical simulations; J.J. and H.Z. designed and performed the experiments; J.J. and C.L. analyzed the data; J.J. wrote the whole paper; C.C. checked and improved the overall paper.

Funding: This research was funded by the Foundation for Distinguished Young Talents in Higher Education of Guangdong Province, China (NO. 2017KQNCX004), the Natural Science Foundation of Guangdong Province, China (NO. 2018A030310378) and the China Postdoctoral Science Foundation (NO. 2017M622696).

Conflicts of Interest: The authors declare no conflicts of interest.

References

1. Korvin-Kroukovsky, B.V.; Jacobs, W.R. Pitching and heaving motion of a ship in regular waves. *Trans. Soc. Naval Archit. Mar. Eng. (SNAME)* **1957**, *65*, 590–632.
2. Salvesen, N.; Tuck, E.O.; Faltinsen, O.M. Ship motions and sea loads. *Trans. Soc. Naval Archit. Mar. Eng. (SNAME)* **1970**, *78*, 1–30.
3. Sen, D. Time domain computation of large amplitude 3D ship motion with forward speed. *Ocean Eng.* **2002**, *29*, 973–1002. [CrossRef]
4. Faltinsen, O.M.; Zhao, R. Numerical predictions of ship motions at high forward speed. *Philos. Trans. Phys. Sci. Eng.* **1991**, *334*, 241–252.
5. Harding, R.D.; Hirdaris, S.E.; Miao, S.H.; Pittilo, M.; Temarel, P. Use of Hydroelasticity Analysis in Design. In Proceedings of the 4th International Conference on Hydroelasticity in Marine Technology, Wuxi, China, 10–14 September 2006; pp. 1–12.
6. Heller, S.R.; Abramson, H.N. Hydroelasticity: A new naval science. *J. Am. Soc. Naval Eng.* **1959**, *71*, 205–209. [CrossRef]
7. Lu, D.; Fu, S.; Zhang, X.; Guo, F.; Gao, Y. A method to estimate the hydroelastic behaviour of VLFS based on multi-rigid-body dynamics and beam bending. *Ships Offshore Struct.* **2016**, 1–9. [CrossRef]
8. Bishop, R.E.D.; Price, W.G. *Hydroelasticity of Ships*; Cambridge University Press: Cambridge, UK, 1979.
9. Betts, C.V.; Bishop, R.E.D.; Price, W.G. The symmetric generalized fluid forces applied to a ship in a seaway. *Trans. RINA* **1977**, *119*, 265–278.
10. Price, W.G.; Wu, Y.S. Hydroelasticity of marine structures. *Theor. Appl. Mech.* **1985**, *316*, 311–337.
11. Hirdaris, S.E.; Temarel, P. Hydroelasticity of ships: Recent advances and future trends. *Proc. Inst. Mech. Eng. Part M J. Eng. Marit. Environ.* **2009**, *223*, 305–330. [CrossRef]
12. Hirdaris, S.E.; Lee, Y.; Mortola, G.; Incecik, A.; Turan, O.; Hong, S.Y.; Temarel, P. The influence of nonlinearities on the symmetric hydrodynamic response of a 10,000 TEU Container ship. *Ocean Eng.* **2016**, *111*, 166–178. [CrossRef]

13. Mortola, G.; Incecik, A.; Turan, O.; Hirdaris, S.E. Non linear analysis of ship motions and loads in large amplitude waves. *Trans. Royal Inst. Naval Archit. Part A2 Int. J. Marit. Eng.* **2011**, *153*, 81–87.
14. Cheng, Y.; Okada, T.; Kobayakawa, H.; Miyashita, T.; Nagashima, T.; Neki, I. Simulation of whipping response of a large container ship fitted with a linear generator on board in irregular head seas. *J. Mar. Sci. Technol.* **2018**, *23*, 706–717. [CrossRef]
15. Lee, Y.; White, N.; Wang, Z.; Zhang, S.; Hirdaris, S.E. Comparison of springing and whipping responses of model tests with predicted nonlinear hydroelastic analyses. *Int. J. Offshore Polar Eng.* **2012**, *22*, 1–8.
16. Li, H.; Wang, D.; Liu, N.; Zhou, X.; Ong, M.C. Influence of linear springing on the fatigue damage of ultra large ore carriers. *Appl. Sci.* **2018**, *8*, 763. [CrossRef]
17. Hong, S.Y.; Kim, B.W. Experimental investigations of higher-order springing and whipping-WILS project. *Int. J. Nav. Archit. Ocean Eng.* **2014**, *6*, 1160–1181. [CrossRef]
18. Kim, J.H.; Kim, Y.; Korobkin, A. Comparison of fully coupled hydroelastic computation and segmented model test results for slamming and whipping loads. *Int. J. Nav. Archit. Ocean Eng.* **2014**, *6*, 1064–1081. [CrossRef]
19. Southall, N.; Choi, S.; Lee, Y.; Hong, C.; Hirdaris, S.; White, N. Impact Analysis Using CFD—A Comparative Study. In Proceedings of the Twenty-fifth (2015) International Ocean and Polar Engineering Conference, Kona, HI, USA, 21–26 June 2015; pp. 692–698.
20. Xu, J.; Sun, Y.; Li, Z.; Zhang, X.; Lu, D. Analysis of the hydroelastic performance of very large floating structures based on multimodules beam theory. *Math. Probl. Eng.* **2017**, 1–14. [CrossRef]
21. Chen, Z.Y.; Jiao, J.L.; Li, H. Time-domain numerical and segmented ship model experimental analyses of hydroelastic responses of a large container ship in oblique regular waves. *Appl. Ocean Res.* **2017**, *67*, 78–93. [CrossRef]
22. Kara, F. Time domain prediction of hydroelasticity of floating bodies. *Appl. Ocean Res.* **2015**, *51*, 1–13. [CrossRef]
23. Rajendran, S.; Vasquez, G.; Soares, C.G. Effect of bow flare on the vertical ship responses in abnormal waves and extreme seas. *Ocean Eng.* **2016**, *124*, 49–436. [CrossRef]
24. Wang, S.; Soares, C.G. Experimental and numerical study of the slamming load on the bow of a chemical tanker in irregular waves. *Ocean Eng.* **2016**, *111*, 369–383. [CrossRef]
25. Kim, J.H.; Kim, Y. Prediction of extreme loads on ultra-large containerships with structural hydroelasticity. *J. Mar. Sci. Technol.* **2018**, *23*, 253–266. [CrossRef]
26. Jiao, J.; Zhao, Y.; Ai, Y.; Chen, C.; Fan, T. Theoretical and Experimental Study on Nonlinear Hydroelastic Responses and Slamming Loads of Ship Advancing in Regular Waves. *Shock Vib.* **2018**, *2018*, 1–26. [CrossRef]
27. Soares, C.G.; Fonseca, N.; Pascoal, R. Long term prediction of non-linear vertical bending moments on a fast monohull. *Appl. Ocean Res.* **2004**, *26*, 288–297. [CrossRef]
28. Baarholm, G.S.; Moan, T. Estimation of nonlinear long-term extremes of hull girder loads in ships. *Mar. Struct.* **2000**, *13*, 495–516. [CrossRef]
29. Wu, M.K.; Hermundstad, O.A. Time-domain simulation of wave-induced nonlinear motions and loads and its applications in ship design. *Mar. Struct.* **2002**, *15*, 561–597. [CrossRef]
30. International Association of Classification Societies (IACS). *Unified Requirements S11*; Longitudinal Strength Standard; IACS: London, UK, 2015.
31. Mohammed, E.A.; Benson, S.D.; Hirdaris, S.E.; Dow, R.S. Design safety margin of a 10,000 TEU container ship through ultimate hull girder load combination analysis. *Mar. Struct.* **2016**, *46*, 78–101. [CrossRef]
32. China Classification Society (CCS). *Guidelines for Influence of Springing and Whipping Loads on Hull Girder Fatigue Strength*; CCS: Beijing, China, 2015.
33. Bureau Veritas (BV). *Rules for the Classification of Military Ships*; Part B-Hull and Stability; BV: Paris, France, 2003.